CHEMISTRY
A EUROPEAN JOURNAL

DOI: 10.1002/chem.201002162

Phototriggering Electron Flow through Re^{I}-modified *Pseudomonas aeruginosa* Azurins

Ana María Blanco-Rodríguez,[a] Angel J. Di Bilio,[b] Crystal Shih,[b] Anna Katrine Museth,[b] Ian P. Clark,[c] Michael Towrie,[c] Andrea Cannizzo,[d] Jawahar Sudhamsu,[e] Brian R. Crane,[e] Jan Sýkora,[f] Jay R. Winkler,*[b] Harry B. Gray,*[b] Stanislav Záliš,*[f] and Antonín Vlček, Jr.*[a, f]

Abstract: The $[Re^{I}(CO)_3$(4,7-dimethyl-1,10-phenanthroline)(histidine-124)(tryptophan-122)] complex, denoted $[Re^{I}$(dmp)(W122)], of *Pseudomonas aeruginosa* azurin behaves as a single photoactive unit that triggers very fast electron transfer (ET) from a distant (2 nm) Cu^{I} center in the protein. Analysis of time-resolved (ps–μs) IR spectroscopic and kinetics data collected on $[Re^{I}$(dmp)(W122)AzM] (in which M = Zn^{II}, Cu^{II}, Cu^{I}; Az = azurin) and position-122 tyrosine (Y), phenylalanine (F), and lysine (K) mutants, together with excited-state DFT/time-dependent (TD)DFT calculations and X-ray structural characterization, reveal the character, energetics, and dynamics of the relevant electronic states of the $[Re^{I}$(dmp)(W122)] unit and a cascade of photoinduced ET and relaxation steps in the corresponding Re–azurins. Optical population of $[Re^{I}$(imidazole-H124)$(CO)_3]$→dmp ^{1}CT states (CT = charge transfer) is followed by around 110 fs intersystem crossing and about 600 ps structural relaxation to a ^{3}CT state. The IR spectrum indicates a mixed $Re^{I}(CO)_3$,A→dmp/π→π*(dmp) character for aromatic amino acids A122 (A = W, Y, F) and $Re^{I}(CO)_3$→dmp metal–ligand charge transfer (MLCT) for $[Re^{I}$(dmp)(K122)AzCu^{II}]. In a few ns, the ^{3}CT state of $[Re^{I}$-(dmp)(W122)AzM] establishes an equilibrium with the $[Re^{I}(dmp^{\bullet-})$-$(W122^{\bullet+})$AzM] charge-separated state, ^{3}CS, whereas the ^{3}CT state of the other Y, F, and K122 proteins decays to the ground state. In addition to this main pathway, ^{3}CS is populated by fs- and ps-W(indole)→Re^{II} ET from ^{1}CT and the initially "hot" ^{3}CT states, respectively. The ^{3}CS state undergoes a tens-of-ns $dmp^{\bullet-}$→$W122^{\bullet+}$ ET recombination leading to the ground state or, in the case of the Cu^{I} azurin, a competitively fast (≈30 ns over 1.12 nm) Cu^{I}→$W^{\bullet+}$ ET, to give $[Re^{I}(dmp^{\bullet-})$-(W122)AzCu^{II}]. The overall photoinduced Cu^{I}→Re(dmp) ET through $[Re^{I}$(dmp)(W122)AzCu^{I}] occurs over a 2 nm distance in < 50 ns after excitation, with the intervening fast ^{3}CT–^{3}CS equilibrium being the principal accelerating factor. No reaction was observed for the three Y, F, and K122 analogues. Although the presence of [Re(dmp)-(W122)AzCu^{II}] oligomers in solution was documented by mass spectrometry and phosphorescence anisotropy, the kinetics data do not indicate any significant interference from the intermolecular ET steps. The ground-state dmp–indole π–π interaction together with well-matched W/$W^{\bullet+}$ and excited-state $[Re^{II}(CO)_3(dmp^{\bullet-})]$/$[Re^{I}(CO)_3(dmp^{\bullet-})]$ potentials that result in very rapid electron interchange and ^{3}CT–^{3}CS energetic proximity, are the main factors responsible for the unique ET behavior of $[Re^{I}$(dmp)(W122)]-containing azurins.

Keywords: density functional calculations · electron transfer · IR spectroscopy · peptides · pi interactions

[a] Dr. A. M. Blanco-Rodríguez, Prof. Dr. A. Vlček, Jr.
Queen Mary University of London
School of Biological and Chemical Sciences
Mile End Road, London E1 4NS (UK)
E-mail: a.vlcek@qmul.ac.uk

[b] Dr. A. J. Di Bilio, Dr. C. Shih, Dr. A. K. Museth, Dr. J. R. Winkler, Prof. Dr. H. B. Gray
Beckman Institute, California Institute of Technology
Pasadena, CA 91125 (USA)
E-mail: winklerj@caltech.edu
hbgray@caltech.edu

[c] Dr. I. P. Clark, Dr. M. Towrie
Central Laser Facility, STFC Rutherford Appleton Laboratory
Chilton, Didcot, Oxfordshire OX11 0QX (UK)

[d] Dr. A. Cannizzo
Laboratoire de Spectroscopie Ultrarapide, ISIC, FSB-BSP
Ecole Polytechnique Fédérale de Lausanne
1015 Lausanne-Dorigny (Switzerland)

[e] Dr. J. Sudhamsu, Prof. Dr. B. R. Crane
Department of Chemistry and Chemical Biology
Cornell University, Ithaca, New York 14853 (USA)

[f] Dr. J. Sýkora, Dr. S. Záliš, Prof. Dr. A. Vlček, Jr.
J. Heyrovský Institute of Physical Chemistry
Academy of Sciences of the Czech Republic
Dolejškova 3, 182 23 Prague (Czech Republic)
E-mail: zalis@jh-inst.cas.cz

Supporting information (including ns TRIR spectra, DFT-calculated and experimental UV/Vis absorption spectra, DFT-calculated IR spectra, and supplementary tables) for this article is available on the WWW under http://dx.doi.org/10.1002/chem.201002162.

Introduction

Kinetics studies of long-range electron transfer (ET) through metallolabeled mutants of a blue copper protein *Pseudomonas aeruginosa* azurin have greatly advanced our understanding of electron-tunneling pathways through peptide β strands,[1–5] as well as at protein interfaces.[6] Theoretical analysis has revealed the roles of molecular fluctuations and multiple interfering tunneling pathways in tuning intraprotein-ET rates in Ru-based azurins.[7,8]

Whereas oxidation of the azurin Cu^{I} center by electronically excited or oxidized metallolabels usually occurs on a μs–ms timescale,[1,2] dramatic ET acceleration into the tens-of-ns range has been observed[9] in an azurin mutant in which a tryptophan (W122) is placed next to a [$Re^{I}(CO)_3$(dmp)] label bound to the imidazole group of H124 (this Re-modified protein is denoted [Re(dmp)(W)AzCu^{I}] (dmp = 4,7-dimethyl-phenanthroline)).[10] To explain these observations a sequential tunneling mechanism was proposed (Scheme 1), in which the ^{3}CT-excited Re label is first reduced by the W122 indole group, followed by a $Cu^{I}\rightarrow W^{\bullet+}$

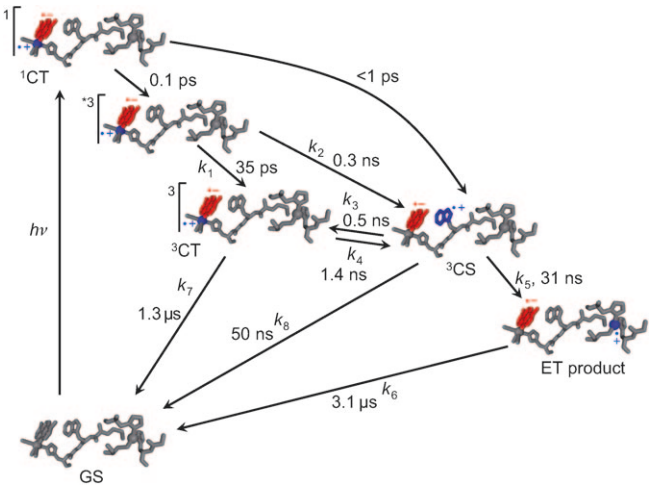

Scheme 1. Photoinduced electron transfer through [Re^{I}(dmp)(W)AzCu^{I}]. Optical population of several ^{1}CT-excited states is followed by a series of relaxation and ET steps. The sites of the excited electron and hole are shown in red and blue, respectively. Lifetime values are pertinent to [Re^{I}(dmp)(W)AzCu^{I}].[9]

ET, effectively splitting the approximately 2 nm ET pathway into two shorter steps.[9] The reaction mechanism involves several relaxation and ET events occurring on timescales ranging from femto- to nanoseconds.

This work has raised important questions about the roles of the [$Re^{I}(CO)_3$(dmp)(W122)] unit and its electronic excited states in the ET mechanism. By replacing the Cu^{I} center with Cu^{II} or Zn^{II}, we remove the long-range charge separation across the Re-labeled azurin (i.e., the 31 ns step in Scheme 1), which isolates the reactive [Re^{I}(dmp)(W)] unit, and focuses on the kinetics and mechanism of the primary ET step from W to the excited Re chromophore. Detailed structural, kinetic, and spectroscopic studies of [Re^{I}(dmp)(W)AzM] (M = Zn^{II}, Cu^{II}, and Cu^{I}) using ps–ns time-resolved IR (TRIR) and emission spectroscopy, combined with a theoretical time-dependent (TD)DFT excited-state analysis, provide a comprehensive picture of [Re^{I}(dmp)(W)] photobehavior and identify factors that make this unit a unique ultrafast ET phototrigger. It emerges that the ET-accelerating role of the tryptophan intermediate goes well beyond the simple splitting of the ET path, with interesting implications for long-range hopping in biological systems, as well as for the design of new molecular schemes for photoinduced charge separation.

Experimental Section

Materials: [Re^{I}(dmp)(A)AzCu^{II}] (A = W, Y, F)[10] were prepared and handled as described previously[9,11] and in the Supporting Information. The [Re^{I}(dmp)(A)AzZn^{II}] samples were made from the corresponding apoprotein by Zn^{II} addition. TRIR experiments were performed in 50 mM Na/KP_i buffer in D_2O (pD ≈ 7.2) at 21 °C. Emission experiments were performed in H_2O, 50 mM NaP_i (pH ≈ 7.1) at 21 °C. Reduction to [Re^{I}(dmp)(A)AzCu^{I}] was accomplished by slow addition of a concentrated solution of sodium dithionite (Aldrich) in 0.5–1.0 μL aliquots into an azurin solution under a nitrogen atmosphere until it turned colorless. TRIR experiments were thus performed in the presence of a small excess of dithionite. The crystallographic structure determination of [Re^{I}(dmp)W122AzCu^{II}] was reported previously,[9] and the coordinates are deposited in the protein data bank (PDB, id 2i7o).

TRIR and luminescence spectroscopy: TRIR measurements and procedures have been described in detail.[12,13] In short, for ps experiments (0–2 ns), the sample solution was excited at 400 nm, using frequency-doubled pulses from a Ti:sapphire laser of ≈150 fs duration (full width at half maximum (FWHM)) and approximately 3 μJ energy, focused at an area ≈200 μm in diameter. TRIR spectra were probed with IR (≈150 fs) pulses obtained by difference-frequency generation. The IR probe pulses cover a 150–200 cm^{-1} spectral range. For ns–μs measurements, the sample was pumped with 355 nm, 0.7 ns FWHM, and probed with electronically synchronized 150 fs IR pulses.[14] The sample solutions were placed in a round dip approximately 0.75 mm deep, drilled into a CaF_2 plate and tightly covered with a polished CaF_2 window. The cell was raster scanned across the area of the dip in two dimensions to prevent laser heating and decomposition of the sample. FTIR spectra measured before and after the experiment demonstrated sample stability.

Emission-lifetime and time-resolved anisotropy measurements were performed using time-correlated single-photon counting (TCSPC) on an IBH 5000 U instrument equipped with a cooled Hamamatsu R3809U-50 microchannel plate photomultiplier, following the procedures described previously.[15] The samples were excited at 370 nm with an IBH NanoLED-11 diode laser (FWHM 100 ps, 500 kHz repetition rate).

TRIR data analysis: TRIR data were analyzed using singular value decomposition (SVD) followed by fitting to a multiexponential kinetics equation[16,17] implemented (EPFL, Switzerland) in the WaveMetrics IGOR Pro software tool. In brief, this analysis allows us to separate the stochastic noise from the signal $\Delta A(\tilde{\nu},t)$ and express the latter in terms of P spectral $\varepsilon_i(\tilde{\nu})$ and temporal $c_i(t)$ components [Eq. (1)]:

$$\Delta A(\nu,t) = \sum_{i=1}^{P} \varepsilon_i(\nu) c_i(t) \qquad (1)$$

in which $\Delta A(\tilde{\nu},t)$ is the IR difference absorbance measured at time delay t and wavenumber $\tilde{\nu}$. The $c_i(t)$ components are then fitted simultaneously to the appropriate kinetics equation. Herein, we used a multiexponential kinetics model [Eq. (2)]:

$$c_l(t) = (\sum_{k=1}^{n} A_l e^{-t/\tau_k}) \otimes e^{[-(\frac{t}{0.6\times\Delta_{IRF}})^2]} \quad (2)$$

in which a common set of lifetimes (τ_k) describes the dynamic behavior of all the temporal components. This allows us to rewrite Equation (2) as follows:

$$\Delta A(v,t) = \left(\sum_{k=l}^{n} \mathrm{DAS}_k(v) e^{-t/\tau_k}\right) \otimes e^{[-(\frac{t}{0.6\times\Delta_{IRF}})^2]} \quad (3)$$

in which $\mathrm{DAS}_k(\tilde{\nu})$ is the decay-associated spectrum describing the spectral contribution of the respective decay component with a time constant τ_k. The last term describes convolution with the Gaussian instrument response function. $\Delta_{IRF} = 1$ ps (or 1 ns) was used for ps (or ns) experiments. Elementary rate constants were extracted from an analytical solution of the differential equations describing the kinetics model depicted in Scheme 1.[9]

Electronic structure calculations: The electronic structure of the model fragment $[Re^{I}(CO)_3(phen)(W)]^+$ (Figure 1, bottom) was calculated by DFT methods by using the Gaussian 09 program package,[18] employing the hybrid functionals PBE0,[19,20] M06,[21] and long-range-corrected CAM-B3LYP.[22] For H, C, N, and O atoms, 6-31G* polarized triple-ζ basis sets[23] were used for geometry optimization and vibrational analysis and cc-pvdz correlation-consistent polarized valence double-ζ basis sets[24] were utilized in TDDFT calculations. Quasi-relativistic effective core pseudo-potentials and a corresponding optimized set of basis functions were employed for Re.[25] The solvent was described by a conductor-like polarizable continuum-model (CPCM).[26] Electronic transitions were calculated by the TDDFT method at the ground-state geometry optimized with solvent correction. The structure of the lowest triplet excited state a^3A was optimized by unrestricted Kohn–Sham (UKS) calculations. The triplet excited state calculation is in satisfactory agreement with experimental TRIR spectra in the $\tilde{\nu}$(CO) region. The electron density difference plots were drawn using the GaussView program. $[Re^{I}(CO)_3(phen)(W)]^+$ was chosen as a computational model instead of $[Re^{I}(CO)_3(dmp)(W)]^+$ because of a better convergence of UKS optimizations of some of the excited-state structures. Ground-state PBE0 calculations of $[Re^{I}(CO)_3(dmp)(W)]^+$ and $[Re^{I}(CO)_3(phen)(W)]^+$ yield very similar structural parameters (Table S1 in the Supporting Information), as well as excitation energies (see the Supporting Information, Tables S2a and S2b), closely matching the experimental values.

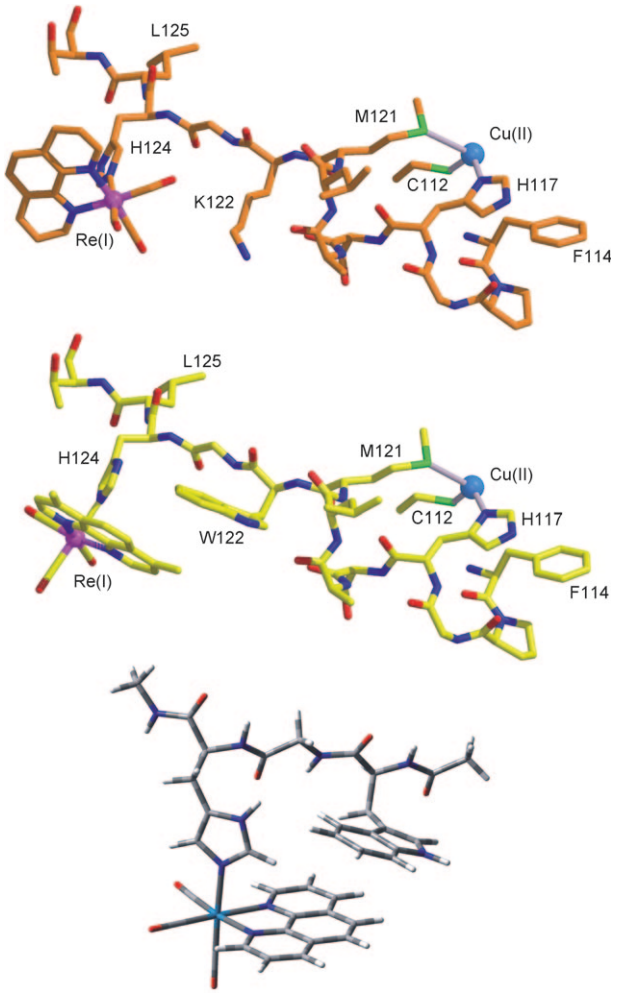

Figure 1. Fragments of the $[Re^{I}(phen)(K)AzCu^{II}]$ (top) and $[Re^{I}(dmp)(W)AzCu^{II}]$ (middle) crystal structures showing the $[Re(CO)_3(N,N)]$ label attached to the imidazole group of H124 and the peptide link to the Cu atom.[9,15] Bottom: Optimized structure of the $[Re^{I}(phen)(W)]^+$ unit used in DFT and TDDFT calculations.

Results

Crystal structures: The crystal structure of $[Re^{I}(dmp)(W)AzCu^{II}]$ (Figure 1) shows that the Re and Cu atoms are 19.4 Å apart. W122 lies between them, at 11.2 Å from Cu and 8.9 Å from Re, as measured to the indole C^{γ} atom. The dmp and W122 aromatic rings slightly overlap, with one dmp methyl group projecting directly over the indole ring; the planes of the respective π systems make a 20.9° angle. The average separation of atoms on the overlapped six-membered rings is 3.82 Å, whereas the W122 indole and the H124 imidazole edges are separated by 4.1 Å. Comparison of the structures of $[Re^{I}(dmp)(W)AzCu^{II}]$ and $[Re^{I}(phen)(K)AzCu^{II}]$ in Figure 1 shows that the orientations of the $[Re(CO)_2(N,N)]$ units (N,N = dmp, phen) relative to the peptide chain and the im(H124) ligand differ by close to 90°. The H124 imidazole ring and the equatorial $[Re(CO)_2(dmp)]$ plane in $[Re^{I}(dmp)(W)AzCu^{II}]$ adopt an unusual orientation, in which the imidazole plane lies close (16°) to the symmetry plane of the equatorial $[Re(CO)_2(dmp)]$ moiety, bisecting the plane of the dmp ligand (Figure 1, middle). In contrast, the plane of the axial ligand is oriented perpendicularly to the symmetry plane, bisecting the equatorial OC–Re–N angles in $[Re^{I}(phen)(K)AzCu^{II}]$ (Figure 1, top) and in other structurally characterized Re–azurins[2,15,27] (with the exception of $[Re^{I}(phen)(H83)AzCu^{II}]$) the small-molecule analogue[28] $[Re^{I}(im)(CO)_3(phen)]^+$, and various complexes $[Re^{I}(R\text{-}py)(CO)_3(N,N)]^+$ (N,N = phen, bpy).[29–33]

Figure 2 shows that $[Re^{I}(dmp)(W)AzCu^{II}]$ is a dimer with twofold symmetry in the crystal; the dominant interactions between neighboring molecules involve the dmp ligands, which cover each other on their outside faces. Unlike the hooking interactions that interdigitate the phen moieties in $[Re^{I}(dmp)(H107)AzCu^{II}]$ (PDB code 1i53)[11,15,34] and $[Re^{I}(phen)(K)AzCu^{II}]$ (PDB code 2i7s)[15] crystals, the $[Re^{I}(dmp)(W)AzCu^{II}]$ dmp ligands are not constrained by the axial H124 and thus can align to a greater extent. One six-membered dmp ring directly stacks with one from a neigh-

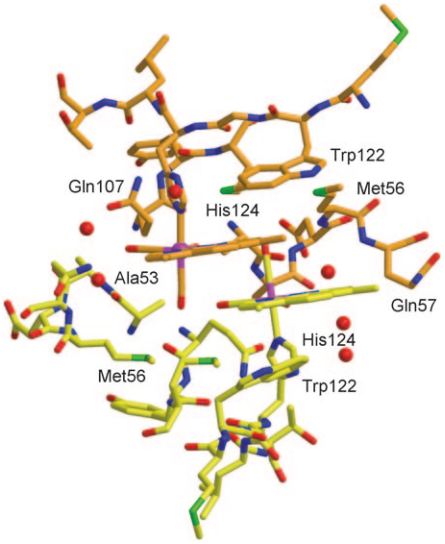

Figure 2. Structure of [Re^{I}(dmp)(W)AzCu^{II}] in the metallolabel region. The red spheres represent water molecules.

boring complex. A four-centered weakly interacting W122···dmp···dmp···W122 stack is apparent in the dimer structure. The Re(CO)$_3$ unit makes van der Waals contacts with the peptide chains: one equatorial carbonyl ligand abuts the methyl side chain of Ala53, whereas the other is within 3.6 Å of the Gln107 side chain. The axial carbonyl points towards an adjacent molecule in the lattice and is within 4.0 Å of the sulfur atoms of both Met109 and Met56 side chains. The axial carbonyl would point away from the protein surface in a solvated monomer in solution.

Solution structures: Solution IR spectra in the region of CO stretching vibrations, υ(CO) (Figure 3), show the same pattern for all three [Re^{I}(dmp)(A)AzM^{II}] complexes: a sharp band due to the in-phase A′(1) vibration at 2028 cm^{-1}; and a broad band at approximately 1917 cm^{-1} that corresponds to

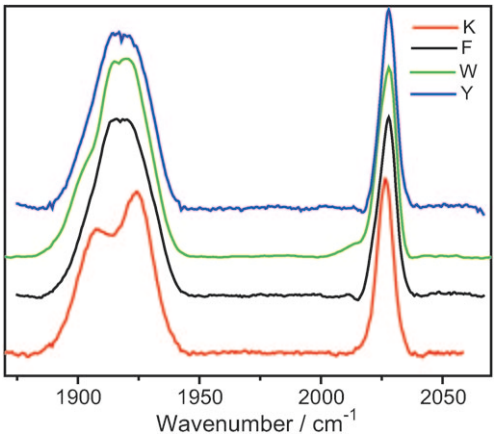

Figure 3. Ground-state FTIR spectra of [Re^{I}(dmp)(A)AzCu^{II}] (A = W, F), [Re^{I}(dmp)(Y)AzZn^{II}] (Y), and [Re^{I}(phen)(K)AzCu^{II}] (K) in a KP$_i$ (D$_2$O, pD ≈ 7.1) buffer.

quasi-degenerate out-of-phase A′(2) and equatorial asymmetric A″ vibrations. In the IR spectrum of [Re^{I}(phen)(K)AzCu^{II}], the A′(2) and A″ bands are split at 1907 and 1924 cm^{-1}, respectively (the symmetry labels assume C_s local symmetry; the assignment is based on previous work[35,36] and the DFT calculations reported below.) We conclude from the IR spectra that all the [Re(dmp)(A)AzM^{II}] proteins containing a 122 aromatic amino acid have the same Re-site solution structure, different from [Re^{I}(phen)(K)AzCu^{II}]. The A′(2)+A″ bandshapes indicate that the three CO ligands reside in a much more diverse environment in [Re^{I}(phen)(K)AzCu^{II}] than in [Re^{I}(dmp)(A)AzM^{II}]. Accordingly, the crystal structures show large asymmetry between the two equatorial CO ligands in [Re^{I}(phen)(K)AzCu^{II}], in which one equatorial CO ligand is directed at Lys122 and Gln107 and the other is solvated, unlike [Re^{I}(dmp)(W)AzCu^{II}], in which both equatorial CO ligands point against an aliphatic side chain of the same molecule.

Laser-induced liquid beam ion desorption mass spectra (LILBID-MS) obtained from aqueous (20 mM NaP$_i$, pH ≈7.0) solutions of [Re^{I}(dmp)(W)AzCu^{II}] clearly show the presence of higher azurin oligomers, especially at higher concentrations, 1–3 mM.[37] Oligomers also are indicated by relatively high values of protein rotation times t_2 that were determined from the biexponential emission anisotropy decay of [Re^{I}(dmp)(W)AzCu^{II}] in NaP$_i$ (20 mM), pH ≈7.1 (3.7 mM: $t_1 = 5.1 \pm 4.3$ ns (18%), $t_2 = 31.5$ (82%); 0.37 mM: $t_1 = 5.1 \pm 3.4$ ns (36%), $t_2 = 16.5 \pm 3.5$ ns (64%)) and [Re^{I}(dmp)(Y)AzZn^{II}] in Na/KP$_i$ (50 mM), D$_2$O, pD ≈7.1 (4.4 mM: $t_1 = 4.8 \pm 0.7$ ns (32%), $t_2 = 50 \pm 2$ ns (68%); 0.44 mM: $t_1 \approx 1$ ns, $t_2 = 30 \pm 1$ ns (45%)). At the same time, the t_1 values are attributable to Re(dmp)–chromophore motions relative to the peptide, which are slower than those[15] in Re–azurins that do not contain an aromatic amino acid next to the Re label.

Photoinduced electron transfer: TRIR spectra and emission decay: TRIR spectroscopy is the technique of choice for the study of excited-state behavior of metal carbonyls because the CO stretching vibrations sensitively respond to changes in electronic and molecular structure,[38] as well as to the relaxation dynamics of the molecular environment following photoexcitation.[15] The IR spectra were measured at selected ps time delays after 400 nm excitation directed to the low-energy part of the Re(CO)$_3$→dmp MLCT absorption band, (see the Supporting Information, Figure S1, bottom). By exciting into the red part of the band we have avoided additional vibrational excitation. Excitation at 355 nm close to the MLCT band maximum was used (for instrumental reasons) in nanosecond experiments. Spectra measured at 355 and 400 nm overlapped in the 1–2 ns time range, in which either instrumental setup can be used, excluding any specific excitation-wavelength effects on the nature of the populated excited states and their reactivity.

For [Re^{I}(dmp)(Y)AzZn^{II}], [Re^{I}(dmp)(Y)AzCu^{II}], and [Re^{I}(dmp)(F)AzCu^{II}], TRIR spectra show only the negative

bleach bands due to ground-state depletion and three upshifted bands attributable[15,27,35,38–43] to a $Re(CO)_3 \rightarrow$dmp ^{3}CT state, approximately described as [$Re^{II}(dmp^{\bullet-})$(A)AzM] (Figure 4 and the Supporting Information, Figure S2). The

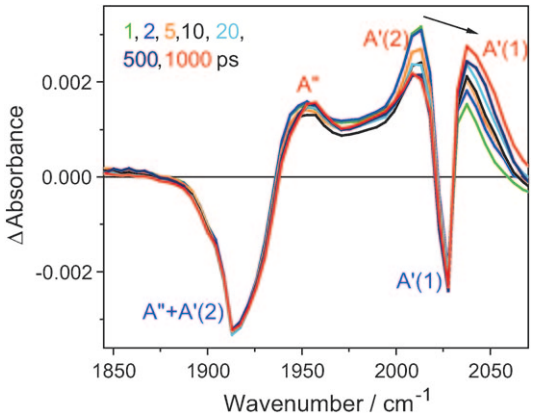

Figure 4. Picosecond TRIR spectra of [Re^I(dmp)(Y)AzZn^{II}] measured at selected time delays after 400 nm, ≈150 fs excitation. Positive and negative bands correspond to excited-state and bleached ground-state absorptions, respectively. The experimental points are separated by 4–5 cm^{-1}. The black arrow shows the dynamical evolution of the excited-state A′(1) band shifting with time from about 2014 to 2039 cm^{-1}. The ground-state band occurs at 2029 cm^{-1}. Virtually identical TRIR spectra were obtained for 1.9 mM solutions of [Re^I(dmp)(Y)AzCu^{II}] and [Re^I(dmp)(F)AzCu^{II}] in 50 mM KP_i buffer in D_2O (pD≈7.0) at 21 °C. See the Supporting Information, Figure S2 for the ns TRIR.

excited-state IR features undergo a small ps–ns upshift due to[15] relaxation processes (Figure 4). On a longer timescale, the transient- and bleach-bands decay with virtually identical kinetics (Supporting Information, Figure S2), demonstrating that the ^{3}CT state decays directly to the ground state. A ^{3}CT lifetime of 1.36±0.17 μs determined (TRIR) for [Re^I(dmp)(Y)AzZn^{II}] is close to the [Re^I-(dmp)(F)AzCu^I] emission lifetime of 1.3 μs.[9] [Re^I-(dmp)(F)AzCu^{II}] (1 mM in H_2O, 50 mM NaP_i; pH≈7.1) shows triexponential emission decay with lifetimes of 3.5± 0.3 (12%), 76.0±2.6 (32%), and 344±10 ns (55%). The longest decay component corresponds to the ^{3}CT population decay, whereas structural relaxation dynamics and/or oligomerization could account for the shorter kinetics components. The shorter excited-state lifetime in Cu^{II} (as compared with Zn^{II}) azurins is attributed to ^{3}CT$\rightarrow Cu^{II}$ energy transfer,[44–46] since $dmp^{\bullet-} \rightarrow Cu^{II}$ ET is excluded by the absence of TRIR signals that would accompany the production of [$Re^{II}(CO)_3$(dmp)]; the oxidation of the excited Re-label complex ($E' \approx -0.9$ V)[28] by Cu^{II} in azurin (+0.31 V) is thermodynamically possible but presumably slow because of the long distance and large reorganization energy on the Re side.

TRIR spectra (Figure 5) of [Re^I(dmp)(W)AzM] (M= Zn^{II}, Cu^{II}, Cu^I) exhibit the typical three upshifted bands due to the ^{3}CT state, together with a broad band at about 1885 cm^{-1} and a sharp band at about 2004 cm^{-1} that are as-

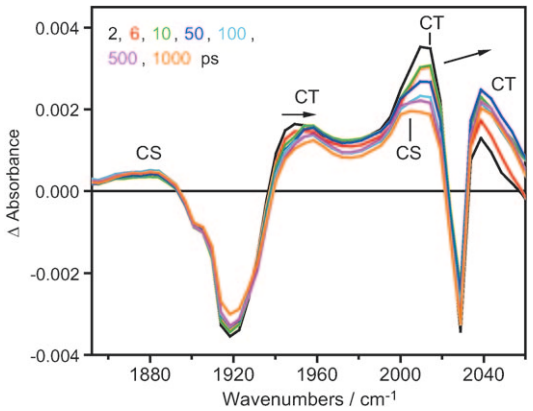

Figure 5. Picosecond TRIR spectra of [Re^I(dmp)(W)AzZn^{II}] measured at selected time delays (in ps) after 400 nm, ≈150 fs excitation. Experimental points are separated by 4–5 cm^{-1}. The arrows show the relaxation-related ^{3}CT band shifts (the small ^{3}CS rise is apparent only after background subtraction). Solution in 50 mM KPi buffer in D_2O (pD≈7.0) at 21 °C.

signed to the A″+A′(2) and A′(1) vibrations, respectively, of the W(indole)$\rightarrow$[$Re(CO)_3$(dmp)] ^{3}CS state, [$Re^I(dmp^{\bullet-})$-($W^{\bullet+}$)AzM]; hereafter, these sets of IR bands will be abbreviated to ^{3}CT and ^{3}CS bands, respectively. The ^{3}CS band assignment is based on the similarity with IR spectra of [Re^I-(*N*-L)$(CO)_3$(bpy$^{\bullet-}$/phen$^{\bullet-}$)] (*N*-L=nitrogen-donor ligand such as MeCN, picoline, or pyridine) generated either electrochemically[47–49] or photochemically[38,48,50,51] by intramolecular electron transfer. Whereas the spectral pattern consisting of ^{3}CT and ^{3}CS bands is very similar for all three [Re^I(dmp)(W)AzM] (M=Zn^{II}, Cu^{II}, Cu^I) derivatives, the kinetics and ^{3}CS yields depend on the metal (M). Temporal evolution of TRIR spectra of the individual [Re^I-(dmp)(W)AzM] systems in ps and ns–μs time ranges are described in terms of exponential lifetimes and their corresponding decay associated spectra (DAS) [Eq. (3)], obtained by SVD analysis/global fitting. Comparable kinetics data were obtained on different samples of each azurin and using variations of the fitting procedure. For M=Cu^{II} and Cu^I, the results obtained on 3, 4, and 1.7 mM samples are the same within experimental accuracy. The resultant TRIR and emission-lifetime data are summarized in Table 1.

[*Re^I(dmp)(W)AzZn^{II}*]: The IR bands of the ^{3}CT state are fully developed within the experimental time resolution of around 1 ps, undergoing relaxation-related dynamic upshifts in about the first 1.5 ns (Figure 5). The ^{3}CS band at about 1885 cm^{-1} is also apparent at 1–2 ps, increasing in intensity by around 60% during the first 30–50 ps.

In the ns range, formation of both ^{3}CT and ^{3}CS transients appears to be complete within the 0.7 ns excitation pulse, followed by biexponential decay with low-amplitude 18 ns and principal 157 ns kinetics components, the former involving some 1885 cm^{-1} band-shape changes (Figure 6). A very small ^{3}CT population persists on a longer timescale, after the ^{3}CS bands had disappeared (see the 500 and 1000 ns ex-

Table 1. Exponential time constants of TRIR spectral evolution and emission decay of [Re(dmp)(W)AzM]. Kinetics data obtained from solutions in 50 mM KP_i buffer in D_2O (pD ≈ 7.0) at 21 °C.

[Re(dmp)(W)AzM]	M = Zn^{II}	M = Cu^{II}	M = Cu^{II} emission[c]	M = Cu^{I} TRIR	M = Cu^{I} emission[e]
ultrafast CS rise/CT decay	< 1 ps	< 1 ps		< 1 ps	
relaxation[a]	–	4–5 ps		3–4 ps	
CS rise/CT decay relaxation	≤ 50 ps	100–270 ps	2.9 ± 0.1 ns[d]	40–100 ps	350 ps
CS rise/CT decay	–	4–8 ns	19 ± 1 ns	1.6 ns	
CS rise/CT decay	–	–	–	8 ± 1.6 ns	
CS rise/CT decay	–	–	–	27 ± 7 ns	25 ns
CS + CT decay	18 ± 4 ns 157 ± 7 ns[a]	40–60 ns	63 ± 1 ns	–	
CS decay		1.0–1.5 μs[b]		330 ± 172 ns 3.6 ± 0.3 μs	

[a] Additional very weak ^{3}CT signal is present, decaying with τ of 1.3 μs. [b] Very weak residual signal. [c] 1.9 mM solution in H_2O, 50 mM NaP_i (pH ≈ 7.1). [d] Likely due to dynamic Stokes shift. [e] From ref. [9].

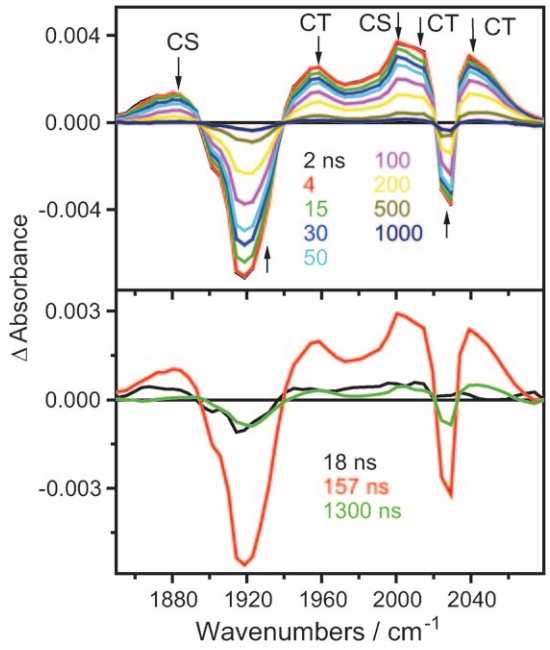

Figure 6. Top: Nanosecond TRIR spectra of [Re^{I}(dmp)(W)AzZn^{II}] (4.4 mM) measured at selected time delays (in ns) after 355 nm, ≈ 0.7 ns excitation. Experimental points are separated by 4–5 cm^{-1}. Bottom: DAS obtained by SVD/global fitting. The 1300 ns lifetime was fixed in the analysis, based on [Re^{I}(dmp)(Y)AzZn^{II}] emission decay. The spectra evolve in the direction of the arrows. Solution in 50 mM KP_i buffer in D_2O (pD ≈ 7.0) at 21 °C.

perimental traces and the 1300 ns DAS that copies the ^{3}CT spectrum, Figure 6).

[*Re^{I}(dmp)(W)AzCu^{II}*]: Picosecond TRIR spectra show both the ^{3}CT and ^{3}CS states being formed within the first ps after excitation (Figure 7, left panel). The temporal evolution on the ps timescale consists of band shifts, width narrowing, and intensity variations that make it hard to distinguish population changes from relaxation effects. To address this matter, we have performed separate SVD/global fitting analyses in the full spectral range in which the relaxation strongly manifests itself by spectral shifts above about 1980 cm^{-1}, and in the 1843–1972 cm^{-1} range, in which population changes prevail. These analyses have identified 4–5 and about 110 ps upshifts of the ^{3}CT A″ and A′(1) bands. The latter component slows to 220–300 ps when fitted over the whole spectral range. The negative DAS in the region of the ^{3}CS 1885 cm^{-1} band and at about 2004 cm^{-1}, together with the relatively large positive DAS amplitudes corresponding to hot ^{3}CT bands, indicate that

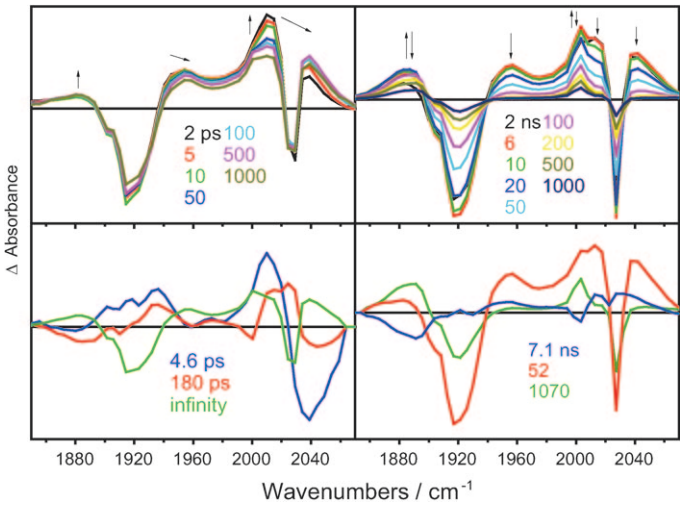

Figure 7. Top: TRIR spectra of [Re^{I}(dmp)(W)AzCu^{II}] measured in the ps time range after 400 nm, ≈ 150 fs excitation (left panel) and the ns range after 355 nm, ≈ 0.7 ns excitation (right panel). The spectra evolve in the direction of the arrows. Bottom: DAS spectra corresponding to kinetics components of 4.6 ± 1.1, and 180 ± 90 ps (left panel); 7.1 ± 1, 52.3 ± 6.5, and 1069 ± 142 ns (right panel). The "infinity" DAS results from extrapolation of the ps measurement to long time delays, which corresponds approximately to an early-ns spectrum. Solution in 50 mM KP_i buffer in D_2O (pD ≈ 7.0) at 21 °C.

the ps relaxation processes are accompanied by conversion of the ^{3}CT state to ^{3}CS, the IR features of which become more pronounced in the 100–300 ps range. On the nanosecond scale (Figure 7, right panel), there is a major 4–8 ns ^{3}CS rise/^{3}CT decay followed by a common 40–60 ns decay of both ^{3}CS and ^{3}CT states. Whereas ^{3}CT bands decay completely, a weak, long-lived (1000–1500 ns) ^{3}CS signal persists. In addition to intensity changes, the ^{3}CS band at about 1885 cm^{-1} undergoes a small upshift to about 1892 cm^{-1} that is complete in 150–200 ns.

[*Re(dmp)(W)AzCu^{I}*]: TRIR spectra (Figure 8) show qualitatively the same pattern as that of the Cu^{II} species, albeit with much stronger ^{3}CS bands. The ^{3}CT state and part of the ^{3}CS population are formed within the 1 ps experimental

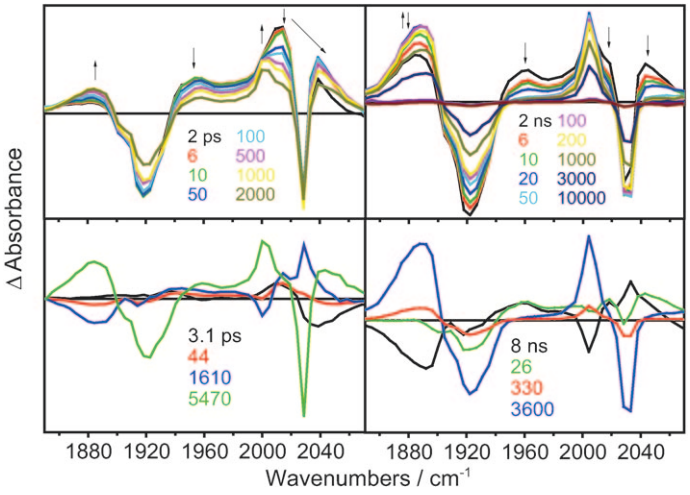

Figure 8. Top: TRIR spectra of [Re^{I}(dmp)(W)AzCu^{I}] measured in the ps time range after 400 nm, ≈150 fs excitation (left panel) and the ns range after 355 nm, ≈0.7 ns excitation (right panel). Bottom: DAS spectra corresponding to kinetics components specified in Table 1. The 5470 ps DAS (bottom left, green) results from extrapolation to long time delays, which corresponds approximately to an early-ns spectrum.

resolution. Further picosecond spectral time evolution consists of a 3–4 ps upshift of the ^{3}CT bands, followed by a 40–100 ps ^{3}CT upshift and small decay, combined with a ^{3}CS rise. On the nanosecond scale, the ^{3}CS rise and ^{3}CT decay continue with time constants of 1.6 ns (determined from the ps experiment), 8 ns (major), and 27 ns (minor). The latter is manifested by a rise mostly of the high-energy side of the 1885 cm^{-1} band and a ^{3}CT decay. The 27 ns process leaves only the ^{3}CS product that decays with minor 330 ns and major 3.6 μs kinetics components. As is the case for the Cu^{II} species, there is a small upshift and a change in shape of the 1885 cm^{-1} ^{3}CS band after 150–200 ns.

TRIR spectra also were measured from solutions of [Re(dmp)(Y)AzZn^{II}], [Re(dmp)(Y)AzCu^{II}], and [Re(dmp)(F)AzCu^{II}] in the presence of a large excess of $Na_2S_2O_4$. TRIR bands of [Re^{I}(dmp$^{\bullet-}$)(Y)AzM] (M = Zn^{II}, Cu^{I}) are formed at about 1885 and 2004 cm^{-1} with lifetimes of hundreds-of-ns. The absence of such long rise kinetics in TRIR measurements on [Re(dmp)(W)AzCu^{I}] excludes any possible contamination from ^{3}CT quenching by sodium dithionite in solution.

Electron transfer kinetics and mechanism: The spectroscopic and kinetics data for [Re^{I}(dmp)(W)AzM] are consistent with the mechanism outlined in Scheme 1 for [Re^{I}(dmp)(W)AzCu^{I}].[9] The long-range ET is shut out in the case of M = Zn^{II}, Cu^{II} ($k_5 = k_6 = 0$), restricting the ET activity to the [Re^{I}(dmp)(W)] moiety. The kinetics data (Table 1) were analyzed using the model shown in Scheme 1,[9] revealing the time ranges of individual reaction steps and estimating values of the ^{3}CT–^{3}CS equilibrium constant K.

[*Re^{I}(dmp)(W)AzZn^{II}*]: The ^{3}CS state is produced in <1 and <50 ps (Figure 5, S2). No ^{3}CT/^{3}CS equilibration is seen on the ns timescale, indicating that ^{3}CS formation occurs only from ^{1}CT and unequilibrated ^{3}CT states. By deconvolution of the ^{3}CT and ^{3}CS spectra and comparing their ratio with [Re^{I}(dmp)(W)AzCu^{II}], K was estimated to be 0.34. The major 157 ns decay component corresponds to the ^{3}CS decay that is in a fast equilibrium with the long-lived (1.36 μs) ^{3}CT state. The minor 18 ns component probably reflects conformational changes in the ^{3}CS state since the corresponding DAS indicates shape changes of the band at about 1885 cm^{-1}.

[*Re^{I}(dmp)(W)AzCu^{II}*]: By using the time constants from Figure 7, we estimate K to be 1.6. The 4–8 ns lifetime (Table 1) reflects ^{3}CT/^{3}CS equilibration, k_3+k_4. ^{3}CS decays (together with ^{3}CT) with about a 60 ns lifetime that is related to k_8. The small residual ^{3}CS signal (apparent in Figure 7, the 1000 ns spectrum and the 1070 ns DAS) that decays with a 1–1.5 μs lifetime is tentatively attributed to the deprotonated species [Re^{I}(dmp$^{\bullet-}$)(W$^{\bullet}$)AzCu^{II}] produced by a slow side reaction from the ^{3}CS state [Re^{I}(dmp$^{\bullet-}$)(W$^{\bullet+}$)AzCu^{II}]. W$^{\bullet+}$ deprotonation is expected to occur with a time constant of 100–200 ns.[52] Consistent with this expectation, the ^{3}CS band at about 1885 cm^{-1} reshapes and shifts to about 1990 cm^{-1} between 50 and 150 ns.

[*Re^{I}(dmp)(W)AzCu^{I}*]: Empirical rate constants determined herein by SVD/global fitting (Table 1) of the TRIR data generally agree with the results of our previous analysis (Scheme 1).[9] The IR spectra of the ^{3}CS state [Re^{I}(dmp$^{\bullet-}$)(W$^{\bullet+}$)AzCu^{I}] and the ET product [Re^{I}(dmp$^{\bullet-}$)(W)AzCu^{II}] are very similar, belonging to the same chromophore, [Re^{I}(CO)$_3$(dmp$^{\bullet-}$)], albeit in a different protein environment. The main 1.6 ns kinetics component corresponds to ^{3}CT/^{3}CS equilibration k_3+k_4 ($K \approx 3$),[9] whereas the 8–9 ns lifetime probably belongs to the same process in a less reactive conformer or an oligomer. The approximately 27 ns kinetics component is related to Cu^{II}→W$^{\bullet+}$ ET in the ^{3}CS state (k_5), because the corresponding DAS indicates reshaping of both ^{3}CS bands. The lifetime of approximately 330 ns could be related to structural changes of the [Re^{I}(dmp$^{\bullet-}$)(W)AzCu^{II}] product. The ground state is regenerated by 3.1–3.6 μs dmp$^{\bullet-}$→Cu^{II} ET (k_6) that is exergonic by approximately 1.8 eV.

Re-label excited-state character and dynamics: TRIR spectra: The Re chromophore in [Re^{I}(dmp)(A)AzM] shows the typical ^{3}CT broad emission band peaking at 540–550 nm and three excited-state ν(CO) IR bands that are shifted to higher wavenumbers relative to the ground-state bands (Figures 4–8 and the Supporting Information, S2). The A″ and A′(2) bands become well separated upon excitation, shifted from their common ground-state value of 1917 cm^{-1} to approximately 1960 and 2014 cm^{-1}, respectively, as observed for other Re^{I}–azurins and Re^{I} carbonyl–diimine complexes.[15,27,35,38–43] The A′(1) bands of [Re(phen)(K)AzCu^{II}]

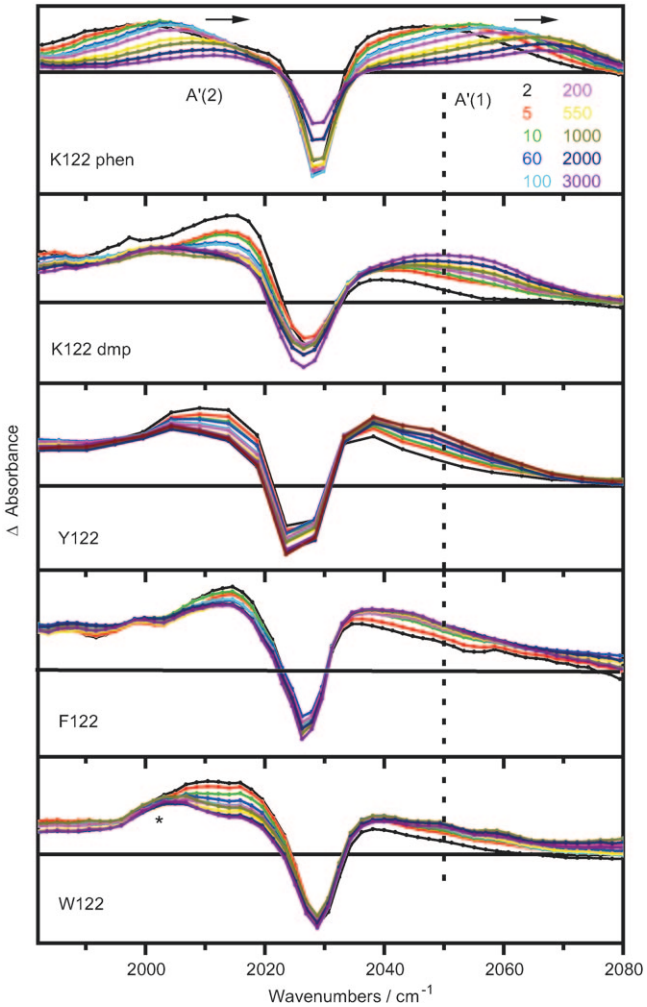

Figure 9. TRIR spectra of [Re(N,N)(A)]-labeled azurins in the high-energy part of the υ(CO) region. From top to bottom: [Re-(phen)(K)AzCu^{II}], [Re(dmp)(K)AzCu^{II}], [Re^{I}(dmp)(Y)AzCu^{II}], [Re^{I}-(dmp)(F)AzCu^{II}], and [Re^{I}(dmp)(W)AzCu^{II}] (3–4 mM in KP$_i$-D$_2$O, pD ≈7.1, 21 °C) measured at selected time delays (see the top panel) after 400 nm, ≈150 fs laser-pulse excitation. The dotted line shows the position of the highest excited-state band of [Re^{I}(dmp)(K)AzCu^{II}]. Experimental points are separated by ≈5 cm^{-1} for [Re^{I}(dmp)(Y)AzCu^{II}] and ≈1.9 cm^{-1} for all others. * = spectral feature due to the ^{3}CS formation.

and [Re(dmp)(K)AzCu^{II}] shift by +38.5 and about +25 cm^{-1}, respectively, on going from the ground state to the relaxed ^{3}CT excited state, indicating a smaller degree of Re(CO)$_3$→N,N charge separation for N,N = dmp. Further differences concern the dynamical behavior of the A′(1) band after excitation (Figure 9). For [Re^{I}(phen)(K)AzCu^{II}], A′(1) undergoes an "instantaneous" (i.e., <1 ps) shift of +9.4 cm^{-1}, followed by a triexponential dynamical upshift with time constants of 2, 7.8, and 539 ps, and a total amplitude of +29 cm^{-1}; the slowest (539 ps) component corresponds to structural motions relocating the Re^{I}-chromophore relative to the peptide chain.[15] The excited-state A′(1) IR band of [Re^{I}(dmp)(K)AzCu^{II}] is much broader; the "instantaneous" shift is slightly negative and the dynamic blue shift is still apparent between 2 and 3 ns, although it cannot readily be quantified. The Re–azurins containing aromatic amino acids at position 122 show a common excited-state IR pattern that is different from that of [Re^{I}-(dmp)(K)AzCu^{II}] and other Re–azurins (Figure 9).[15] The excited-state A′(1) band partly overlaps with the bleach band and tails toward higher energies. At 1–2 ps after excitation, the A′(1) band is shifted to lower energies by at least −12 cm^{-1}. This negative "instantaneous" shift is followed by a dynamic upshift across the bleach region that is apparent until about 2 ns. The band maximum of the relaxed excited state is upshifted from the ground-state position by only 8–10 cm^{-1} for W122 and 10–13 cm^{-1} for Y122 and F122. The relatively small A′(1) upshift points to a smaller Re(CO)$_3$→dmp MLCT contribution to the excited state if an aromatic amino acid is placed next to the Re chromophore; this conclusion is further supported by DFT and TDDFT calculations below.

Re-label excited-state character and dynamics: Electronic structure calculations: DFT calculations were performed on a model peptide fragment [Re^{I}(phen)(W)]$^+$ with L125 and M121 replaced by CH$_3$NH- and CH$_3$C(O)-, respectively (Figure 1, bottom). The H$_2$O solvent was described by CPCM. Calculations with three different functionals (PBE0, M06, and CAM-B3LYP) were compared, each of which provides an optimized [Re(phen)(W)]$^+$ structure that represents the relevant part of the protein (Figure 1 and the Supporting Information, Table S1). However, M06 overestimates the ground-state W(indole)–phen interaction, which results in the distances and the angle between the indole and phen planes being too small. The long-range corrected B3LYP functional (CAM-B3LYP) reproduces well the ground-state structure (see the Supporting Information, Table S1) and models the ^{3}CS state in accordance with the M06 result (see the Supporting Information, Figure S3), but predicts that the lowest allowed electronic transitions are at much higher energies than observed in the experimental absorption spectrum.

According to PBE0, the three LUMOs are localized on phen, whereas the HOMO and HOMO-1 are W122 indole-ring π orbitals (Figure 10). Re d-π orbitals occur slightly lower in energy, as HOMO-2, which contains a large H124-imidazole π contribution; and HOMO-3. The orbitals HOMO-4 and HOMO-5 are π-peptide (W122) orbitals.

TDDFT positions of singlet electronic transitions of [Re^{I}-(phen)(W)]$^+$ are summarized in the Supporting Information (Tables S2–S4). The simulated and experimental spectra are also shown in the Supporting Information (Figure S1). The two lowest transitions calculated (PBE0) at 465 (b^{1}A) and 424 nm (c^{1}A) have W(indole)→phen charge-transfer character, originating in HOMO→LUMO, LUMO+1 excitations, as documented by the accompanying electron-density change shown in Figure 11 (see the Supporting Information, Figure S3 for PBE0 (M06 and CAM-B3LYP) results). Oscillator strengths of these two transitions are very low (Table S2), precluding observation in the spectrum. Other weak W(indole)→phen transitions were calculated around

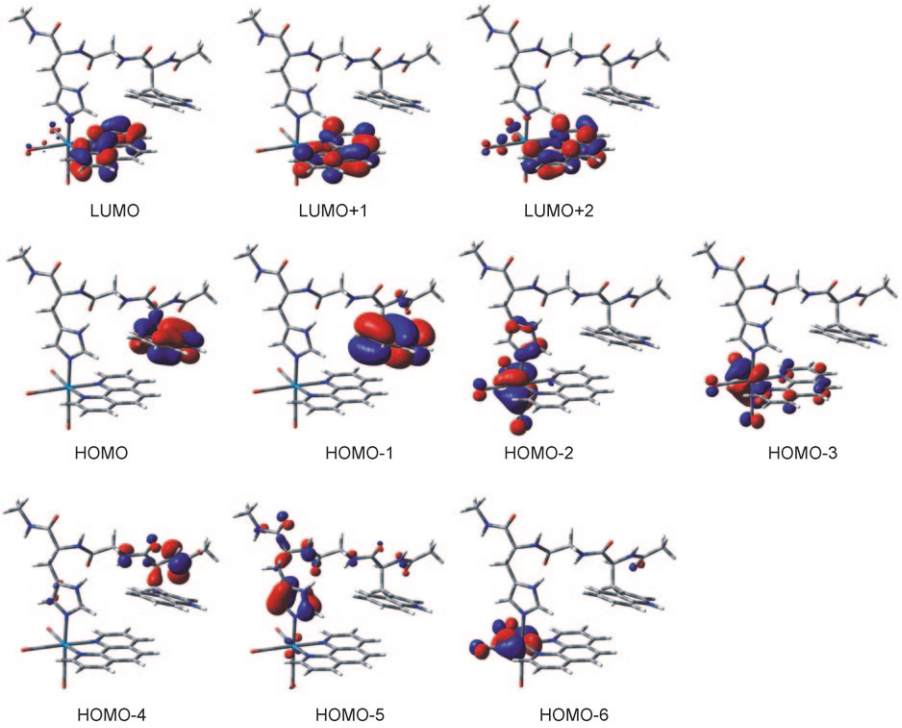

Figure 10. Frontier molecular orbitals of the $[Re^{I}(phen)(W)]^{+}$ fragment calculated by DFT (PBE0, CPCM-H_2O).

phen character, $^{3}[Re^{I}(phen^{\bullet-})(W^{\bullet+})]^{+}$ (Figure 12, top and Table S5 in the Supporting Information). UKS (PBE0/CPCM-H_2O) triplet-state structural optimization identifies the lowest relaxed triplet excited state of $[Re^{I}(phen)(W)]^{+}$ as ^{3}CT, demonstrated by the spin-density distribution (Figure 12). Predicted $\tilde{\nu}$(CO) differences between the ^{3}CT and the ground state of +42 (A″), +75 (A′(2)), and +8 (A′(1)) cm^{-1} agree well with the experimental values of +40, +94, and $\leq$+10 cm^{-1} (see the Supporting Information, Figure S4). The unusually small A′(1) $\tilde{\nu}$(CO) shift is caused by the very small CO electronic depopulation, which is mainly restricted to the axial CO ligand (Figure 12). The extent of $Re^{I}(CO)_3\rightarrow$phen charge transfer in the ^{3}CT state is limited by two effects: admixture

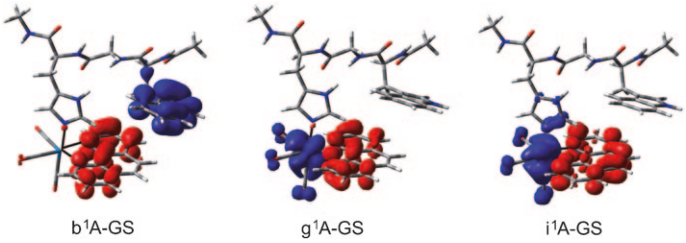

Figure 11. TDDFT (PBE0, CPCM-H_2O)-calculated electron-density difference between the lowest W(indole)→phen ^{1}CT state (left, b^{1}A) and the two optically populated ^{1}CT states (g^{1}A and i^{1}A, see the Supporting Information, Table S2) and the $[Re^{I}(phen)(W)]^{+}$ ground state. Colors show regions where the electron density decreases (blue) and increases (red) upon excitation.

380 nm. Two intense transitions from HOMO-2,3 to LUMO and LUMO+1 calculated at 350 (g^{1}A) and 335 nm (i^{1}A) give rise to the experimentally observed broad 300–400 nm shoulder. Calculated electron-density differences demonstrate their respective predominant $Re^{I}(CO)_3\rightarrow$phen MLCT and mixed $[Re^{I}$(imidazole)$(CO)_3]\rightarrow$phen MLCT/LLCT characters (Figure 11). Both these transitions are excited by 355 and 400 nm laser pulses in the time-resolved spectral experiments. Another intense, predominantly ^{1}CT, transition was calculated at 329 nm.

TDDFT calculations at the ground-state geometry reveals two nearly degenerate triplet states: the charge-transfer state, ^{3}CT, has major $Re^{I}\rightarrow$phen, and minor imidazole→phen, W(indole)→phen, and π→π*(phen) contributions, whereas the charge-separated state, ^{3}CS, has a W(indole)→

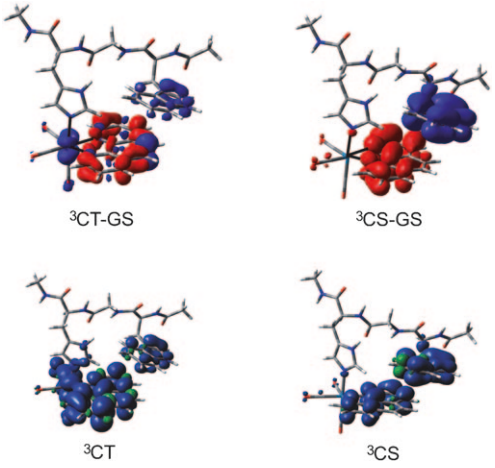

Figure 12. Top: Electron density differences between ^{3}CT- and ^{3}CS states and the ground state at the ground-state geometry calculated by TDDFT (CPCM-H_2O). Bottom: spin density distributions in structurally optimized ^{3}CT and ^{3}CS states (DFT UKS CPCM-H_2O). PBE0 and M06 functionals were used for the ^{3}CT and ^{3}CS calculations, respectively.

of the π–π*(phen) intraligand excitation and partial charge transfer from the W122 indole ring. The similarity of the $[Re^{I}$(dmp)(A)AzM] (A = W,F,Y) TRIR spectra (Figure 9) suggests that the phenol and phenolate groups also donate electron density to dmp in the ^{1}CT excited states of [Re(dmp)(F)AzM] and [Re(dmp)(Y)AzM], respectively. UKS (M06/CPCM-H_2O) predicts that ^{3}CS of a W(indole)→phen character, $^{3}[Re^{I}(phen^{\bullet-})(W^{\bullet+})]^{+}$ (Figure 12), will be the lowest triplet, allowing us to optimize its structure and per-

form vibrational analysis. The ^{3}CS A″+A′(2) $\tilde{\nu}$(CO) vibrations (M06/H_2O, see the Supporting Information, Figure S5) are downshifted from ground-state values by −30 and −23 cm^{-1}, respectively, because of the increased π-electron density on the phen ligand. Indeed, TRIR spectra show bands at about 1885 (A″+A′(2)) and 2004 cm^{-1} (A′(1)), that is about 33 and 26 cm^{-1} lower than corresponding ground-state bands. The sensitivity of the calculated electronic structure of the lowest triplet states to the computational details is in agreement with the experimentally determined energetic proximity of the [Re^I(dmp)(W122)AzCu^I] ^{3}CT and ^{3}CS states, about 0.028 eV.[9] The good match between experimental and calculated excited-state IR spectra demonstrates that UKS, PBE0, and M06 calculations in water provide good models for the ^{3}CT and ^{3}CS states, respectively.

Discussion

The [$Re^I(CO)_3$(dmp)(H124)(W122)] moiety of the azurin mutant emerges from this study as an electronically coupled active site that can be regarded as a single photoactive unit. The X-ray crystal structure (Figure 1) clearly demonstrates an interaction between the nearly parallel W(indole) and dmp rings that is strong enough to rotate the [$Re^I(CO)_3$(dmp)] label relative to its position in [Re^I(dmp)(K)AzCu^{II}] by about 90° and change the orientation of the H124 imidazole ligand relative to the [$Re^I(CO)_3$(dmp)] symmetry plane. DFT calculations and both ground- and excited-state IR spectra indicate that the intramolecular W(indole)-dmp interaction persists in solution. A similar interaction occurs between dmp and F122 (or Y122) in [Re^I(dmp)(F or Y)AzM]. Although azurins, including [Re(dmp)(W)AzCu^{II}], form oligomers in solutions,[37] the kinetics data can be interpreted in terms of intramolecular ET and relaxation steps only. Intraprotein ET is much faster than ET across protein–protein interfaces in oligomers, especially when the proteins are bound by nonspecific forces, as indicated[37] by LILBID mass spectra. Intermolecular ET would not be competitive even if the indole–dmp–dmp–indole interaction found in [Re(dmp)(W)AzCu^{II}] dimers in crystals (Figure 2) were preserved in an oligomer core, since each dmp ligand is coupled to an indole of the same azurin molecule, being separated from that of the second molecule by another [Re(dmp)] unit.

Photoinduced charge-separation to give the [Re^I(dmp$^{\bullet-}$)(W$^{\bullet+}$)AzM] ^{3}CS state involves several ET steps that occur on timescales ranging from fs to a few tens-of-ns (Scheme 1 and Table 1). The ET reactivity can be understood in terms of the electronic structure, energetics and relaxation dynamics of electronic excited states of [Re^I(dmp)(W)]. Optical excitation populates ^{1}CT excited states (*[Re^{II}(dmp$^{\bullet-}$)(W)], Figure 11) that undergo intersystem crossing with a time constant of approximately 110 fs,[16,17,53] producing a hot ^{3}CT state. The approximately 110 fs ^{1}CT lifetime allows for ultrafast exergonic W→Re^{II} ET to produce the ^{1}CS state, followed by fs intersystem crossing to ^{3}CS. This pathway is responsible for sub-ps ^{3}CS formation, observed by TRIR (direct optical excitation into W→dmp ^{1}CS states is improbable because of the very low oscillator strengths of corresponding transitions: see the Supporting Information, Table S2 and Figure S1). The ^{3}CT state is initially "hot": it is both vibrationally excited and in an unequilibrated solvent and protein environment.[15] Relaxation (complete in 1–2 ns, as follows from the dynamical shift of the excited-state A′(1) υ(CO) band) involves a multitude of structural movements, which optimizes the electrostatic interactions between the excited Re label, the peptide, and the solvent molecules.[15] Concomitantly with structural relaxation of the Re site, the hot ^{3}CT state undergoes W→Re^{II} ET to the ^{3}CS state [Re^I(dmp$^{\bullet-}$)(W$^{\bullet+}$)] in tens-to-hundreds of ps, slowing to about 1 ns upon ^{3}CT relaxation. The relaxed ^{3}CT state is the principal precursor of charge separation. Electronic interaction between W(indole) and dmp in the predominantly Re→dmp/π–π*(dmp) ^{3}CT state is evident from calculated electron-density changes and excited-state spin-density distribution that partly extends over the W(indole) moiety (Figure 12). The ^{3}CT to ^{3}CS conversion can be viewed either as a W(indole)→dmp$^{\bullet-}$→Re^{II} electron-density shift or a W→Re^{II} ET mediated by dmp$^{\bullet-}$ (and its π–π interaction with the indole). An alternative ET pathway through peptide bonds is less likely because of much longer length and negligible electronic involvement of peptide and imidazole orbitals in the ^{3}CT state (Figures 10 and 12). DFT calculations show that the relaxed ^{3}CT and ^{3}CS states are nearly isoenergetic. Accordingly, the kinetics analysis points to an equilibrium between these two states, with ^{3}CS only 0.028 (0.012) eV below ^{3}CT for Cu^I (Cu^{II}), whereas ^{3}CS is 0.027 eV above ^{3}CT for Zn^{II}. The [Re^I(dmp$^{\bullet-}$)(W$^{\bullet+}$)AzM] ^{3}CS state decays to the ground state by dmp$^{\bullet-}$→W$^{\bullet+}$ charge recombination, which takes place with a 30–60 ns time constant for Cu^{II} or Cu^I and about 160 ns for Zn^{II}. This is a highly exergonic process (2.0–2.5 V) occurring in the Marcus-inverted region. The ET and relaxation dynamics within [Re^I(dmp)(W)] are similar for Cu^I and Cu^{II}, with the equilibrium constant K being slightly larger for Cu^{II} (3) than Cu^I (1.6). [Re^I(dmp)(W)Zn^{II}] is distinctly different, because the ^{3}CS state is formed only by ultrafast processes in a close-to-equilibrium ratio. W→Re^{II} ET (^{3}CT→^{3}CS) is slightly endergonic ($K \approx 0.34$), in contrast to the Cu^I and Cu^{II} energetics. The different Zn^{II} azurin behavior could be attributable to more extensive oligomerization of [Re^I-(dmp)(Y)Zn^{II}] than [Re^I(dmp)(W)Cu^{II}], as indicated by longer rotation times of approximately 50 and 30 ns, respectively (see above). Oligomerization could shield the binding site and change its structure and energetics by intermolecular interactions. The energetic proximity of the ^{3}CT and ^{3}CS states contrasts with the approximately 0.4 V difference between the Re-label excited-state reduction potential ($E' \approx$ +1.4 V vs. NHE)[28] and the indole oxidation potential ($E' \approx 1.01$ V),[54] suggesting that the binding site energetics are strongly affected by the interaction between dmp indole groups and the protein environment.

The full potential of the [Re^{I}(dmp)(W)] ET phototrigger is revealed by the dramatic acceleration[9] of long-range $Cu^{I}\rightarrow Re^{II}$ ET in ^{3}CT-excited [Re^{I}(dmp)(W)AzCu^{I}]. Cu^{II} formation is complete in a few tens-of-ns, whereas no reaction is found for analogous azurins with phenylalanine or tyrosine at position 122. In the long-range ET mechanism of [Re^{I}(dmp)(W)AzCu^{I}] (Scheme 1), the rapidly established ^{3}CT/^{3}CS equilibrium feeds the productive $Cu^{I}\rightarrow W^{\bullet+}$ ET step from a long-lived ^{3}CT population, whereas the ^{3}CS $dmp^{\bullet-}\rightarrow W^{\bullet+}$ charge recombination is energy wasting, thus decreasing the reaction yield. Productive $Cu^{I}\rightarrow W^{\bullet+}$ ET is remarkably fast, (31 ns) over a 1.12 nm distance, likely because the indole group is electronically well coupled to the peptide. The efficiency of any light-harvesting or photocatalytic system based on this type of mechanism will increase upon increasing the inherent ^{3}CT lifetime, slowing $dmp^{\bullet-}\rightarrow W^{\bullet+}$ recombination, and accelerating the final ET step.

The interaction between W(indole) and dmp is a prerequisite for rapid charge separation in [Re^{I}(dmp)(W)] through the ^{3}CT/^{3}CS equilibrium. Indeed, $W\rightarrow Re^{II}$ ET is much slower in analogous systems without a direct indole-N,N contact. Photoinduced ET reactions in [Re^{I}(pyridine-W)$(CO)_3$(N,N)]$^{+}$ and [Re^{I}(imidazole-W)$(CO)_3$(N,N)]$^{+}$ (N,N = bpy, phen) occur with a time constant of about 30 ns in MeCN solutions, without any ultrafast kinetics component.[14,51] Flash-quench generated [$Re^{II}(CO)_3$(phen)-(H107)]$^{2+}$ oxidizes W108 in [Re$(CO)_3$(phen)-(Q107H)(W48F/Y72F/H83Q/Y108W)AzZn^{II}] with a 360 ns time constant,[34] which is much slower than the similar reaction in ^{3}CT-excited [Re^{I}(dmp)(W)AzM]. The phen and W108 indole rings in these modified proteins are oriented away from each other, therefore disfavoring any direct electronic interaction.

Phototriggering by the [Re^{I}(dmp)(W)] unit in azurins is similar to the 30 ps primary electron transfer in DNA photolyase that occurs over about 1.5 nm involving several π–π interactions: between the W382 indole group and electronically excited flavin radical, whose aromatic rings partly overlap 4.2 Å apart, followed by a "nanowire" of three π–π interacting tryptophans.[55–60] Ultrafast charge-separation is also accomplished in a tight-binding antibody–protein pocket containing *tert*-stilbene π-stacked to tryptophan. Stilbene photoexcitation produces a strongly luminescent ^{1}[stilbene$^{\bullet-}$/$W^{\bullet+}$] charge-separated complex with biosensing functions.[61] This type of π–π interaction can also mediate ET at protein–protein interfaces: fast equilibration between oxidized Zn–porphyrin and a nearby tryptophane has been demonstrated to facilitate charge recombination following photoexcitation of a Zn–cytochrome c peroxidase:cytochrome c complex.[62,63]

We suggest that the principle underlying ET acceleration in [Re^{I}(dmp)(W)AzM] azurins, namely, ultrafast photoinduced charge-separation between a π-stacked electron donor and acceptor, can guide the design and construction of more efficient light-energy harvesting systems. Rhenium carbonyl–diimine/tryptophan assemblies could be exploited in such constructions.

Acknowledgements

We thank Lucie Sokolová (J.W. Goethe University, Frankfurt am Main) for measuring and interpreting the solution LILBID mass spectra. Research at Caltech was supported by the NSF Center for Chemical Innovation (Powering the Planet CHE-0802907 and CHE-0947829) and by NIH (DK019038 to HBG, JRW). The crystallographic work was supported by the NSF-CHE-0749997(BRC). The TRIR and theoretical investigations were funded by the STFC Rutherford Appleton Laboratory, CMSD 43, Queen Mary University of London, European COST D35 and ESF-DYNA programs, and Ministry of Education of the Czech Republic grants ME10124 and OC09043.

[1] R. Langen, I.-J. Chang, J. P. Germanas, J. H. Richards, J. R. Winkler, H. B. Gray, *Science* **1995**, *268*, 1733.
[2] B. R. Crane, A. J. Di Bilio, J. R. Winkler, H. B. Gray, *J. Am. Chem. Soc.* **2001**, *123*, 11623.
[3] A. J. Di Bilio, M. G. Hill, N. Bonander, B. G. Karlsson, R. M. Villahermosa, B. G. Malmström, J. R. Winkler, H. B. Gray, *J. Am. Chem. Soc.* **1997**, *119*, 9921.
[4] L. K. Skov, T. Pascher, J. R. Winkler, H. B. Gray, *J. Am. Chem. Soc.* **1998**, *120*, 1102.
[5] H. B. Gray, J. R. Winkler, *Chem. Phys. Lett.* **2009**, *483*, 1.
[6] C. Gradinaru, B. R. Crane, *J. Phys. Chem. B* **2006**, *110*, 20073.
[7] S. S. Skourtis, I. A. Balabin, T. Kawatsu, D. N. Beratan, *Proc. Natl. Acad. Sci. USA* **2005**, *102*, 3552–3557.
[8] J. J. Regan, J. N. Onuchic, *Adv. Chem. Phys.* **1999**, *107*, 497.
[9] C. Shih, A. K. Museth, M. Abrahamsson, A. M. Blanco-Rodriguez, A. J. Di Bilio, J. Sudhamsu, B. R. Crane, K. L. Ronayne, M. Towrie, A. Vlček, Jr., J. H. Richards, J. R. Winkler, H. B. Gray, *Science* **2008**, *320*, 1760.
[10] The *Pseudomonas aeruginosa* azurin mutants under study have a histidine (H) at position 124 and either tryptophan (W), tyrosine (Y), or phenylalanine (F) at position 122 on the β strand extending from methionine-121 that is coordinated to the metal atom (M = Cu^{I}, Cu^{II}, or Zn^{II}). All other tyrosines and tryptophans are replaced by phenylalanines, and the Re label [$Re^{I}(CO)_3$(dmp)]$^{+}$ (dmp = 4,7-dimethyl-1,10-phenanthroline) is bound to the H124 imidazole. These azurins are denoted [Re^{I}(dmp)(A)AzM] (A = W, Y, F). The symbol A also is used generically for an aromatic amino acid. Lysine (K) analogues used for comparison are denoted [Re^{I}-(dmp)(K)AzCu^{II}] and [Re^{I}(phen)(K)AzCu^{II}] (phen = 1,10-phenanthroline).
[11] A. J. Di Bilio, B. R. Crane, W. A. Wehbi, C. N. Kiser, M. M. Abu-Omar, R. M. Carlos, J. H. Richards, J. R. Winkler, H. B. Gray, *J. Am. Chem. Soc.* **2001**, *123*, 3181.
[12] M. Towrie, D. C. Grills, J. Dyer, J. A. Weinstein, P. Matousek, R. Barton, P. D. Bailey, N. Subramaniam, W. M. Kwok, C. S. Ma, D. Phillips, A. W. Parker, M. W. George, *Appl. Spectrosc.* **2003**, *57*, 367.
[13] A. Vlček, Jr., I. R. Farrell, D. J. Liard, P. Matousek, M. Towrie, A. W. Parker, D. C. Grills, M. W. George, *J. Chem. Soc. Dalton Trans.* **2002**, 701.
[14] M. Towrie, A. W. Parker, A. Vlček, Jr., A. Gabrielsson, A. M. Blanco Rodriguez, *Appl. Spectrosc.* **2005**, *59*, 467.
[15] A. M. Blanco-Rodríguez, M. Busby, K. L. Ronayne, M. Towrie, J. Sýkora, M. Hof, S. Záliš, C. Grădinaru, A. J. Di Bilio, B. R. Crane, H. B. Gray, J. Vlček, *J. Am. Chem. Soc.* **2009**, *131*, 11788.
[16] A. Cannizzo, A. M. Blanco-Rodríguez, A. Nahhas, J. Šebera, S. Záliš, A. Vlček, Jr., M. Chergui, *J. Am. Chem. Soc.* **2008**, *130*, 8967.
[17] A. El Nahhas, A. Cannizzo, F. van Mourik, A. M. Blanco-Rodríguez, S. Záliš, A. Vlček, Jr., M. Chergui, *J. Phys. Chem. A* **2010**, *114*, 6361.
[18] M. J. Frisch, G. W. Trucks, H. B. Schlegel, G. E. Scuseria, M. A. Robb, J. R. Cheeseman, G. Scalmani, V. Barone, B. Mennucci, G. A. Petersson, H. Nakatsuji, M. Caricato, X. Li, H. P. Hratchian, A. F. Izmaylov, J. Bloino, G. Zheng, J. L. Sonnenberg, M. Hada, M. Ehara, K. Toyota, R. Fukuda, J. Hasegawa, M. Ishida, T. Nakajima, Y. Honda, O. Kitao, H. Nakai, T. Vreven, J. A. Montgomery, Jr., J. E. Peralta, F. Ogliaro, M. Bearpark, J. J. Heyd, E. Brothers, K. N.

Kudin, V. N. Staroverov, R. Kobayashi, J. Normand, K. Raghavachari, A. Rendell, J. C. Burant, S. S. Iyengar, J. Tomasi, M. Cossi, N. Rega, J. M. Millam, M. Klene, J. E. Knox, J. B. Cross, V. Bakken, C. Adamo, J. Jaramillo, R. Gomperts, R. E. Stratmann, O. Yazyev, A. J. Austin, R. Cammi, C. Pomelli, J. W. Ochterski, R. L. Martin, K. Morokuma, V. G. Zakrzewski, G. A. Voth, P. Salvador, J. J. Dannenberg, S. Dapprich, A. D. Daniels, O. Farkas, J. B. Foresman, J. V. Ortiz, J. Cioslowski, D. J. Fox, Gaussian 09, Revision A.02, Gaussian, Inc., Wallingford CT, **2009**.

[19] J. P. Perdew, K. Burke, M. Ernzerhof, *Phys. Rev. Lett.* **1996**, *77*, 3865.
[20] C. Adamo, V. Barone, *J. Chem. Phys.* **1999**, *110*, 6158.
[21] Y. Zhao, D. G. Truhlar, *Theor. Chem. Acc.* **2008**, *120*, 215.
[22] T. Yanai, D. P. Tew, N. C. Handy, *Chem. Phys. Lett.* **2004**, *393*, 51.
[23] R. Krishnan, J. S. Binkley, R. Seeger, J. A. Pople, *J. Chem. Phys.* **1980**, *72*, 650.
[24] D. E. Woon, T. H. Dunning Jr. , *J. Chem. Phys.* **1993**, *98*, 1358.
[25] D. Andrae, U. Häussermann, M. Dolg, H. Stoll, H. Preuss, *Theor. Chim. Acta* **1990**, *77*, 123.
[26] M. Cossi, N. Rega, G. Scalmani, V. Barone, *J. Comput. Chem.* **2003**, *24*, 669.
[27] A. M. Blanco-Rodríguez, M. Busby, C. Grădinaru, B. R. Crane, A. J. Di Bilio, P. Matousek, M. Towrie, B. S. Leigh, J. H. Richards, A. Vlček, Jr., H. B. Gray, *J. Am. Chem. Soc.* **2006**, *128*, 4365.
[28] W. B. Connick, A. J. Di Bilio, M. G. Hill, J. R. Winkler, H. B. Gray, *Inorg. Chim. Acta* **1995**, *240*, 169.
[29] L. A. Lucia, K. Abboud, K. S. Schanze, *Inorg. Chem.* **1997**, *36*, 6224.
[30] M. Busby, P. Matousek, M. Towrie, I. P. Clark, M. Motevalli, F. Hartl, A. Vlček Jr. , *Inorg. Chem.* **2004**, *43*, 4523.
[31] D. J. Liard, M. Busby, I. R. Farrell, P. Matousek, M. Towrie, A. Vlček Jr. , *J. Phys. Chem. A* **2004**, *108*, 556.
[32] M. Busby, A. Gabrielsson, P. Matousek, M. Towrie, A. J. Di Bilio, H. B. Gray, A. Vlček Jr. , *Inorg. Chem.* **2004**, *43*, 4994.
[33] L. Wallace, C. Woods, D. P. Rillema, *Inorg. Chem.* **1995**, *34*, 2875.
[34] J. E. Miller, C. Gradinaru, B. R. Crane, A. J. Di Bilio, W. A. Wehbi, S. Un, J. R. Winkler, H. B. Gray, *J. Am. Chem. Soc.* **2003**, *125*, 14220.
[35] D. M. Dattelbaum, K. M. Omberg, J. R. Schoonover, R. L. Martin, T. J. Meyer, *Inorg. Chem.* **2002**, *41*, 6071.
[36] J. Bredenbeck, J. Helbing, P. Hamm, *J. Am. Chem. Soc.* **2004**, *126*, 990.
[37] L. Sokolová, H. Williamson, J. Sýkora, M. Hof, H. B. Gray, B. Brutschy, A. Vlček, Jr., *J. Phys. Chem. B* **2011**, *115*, in press.
[38] D. M. Dattelbaum, K. M. Omberg, P. J. Hay, N. L. Gebhart, R. L. Martin, J. R. Schoonover, T. J. Meyer, *J. Phys. Chem. A* **2004**, *108*, 3527.
[39] M. W. George, F. P. A. Johnson, J. R. Westwell, P. M. Hodges, J. J. Turner, *J. Chem. Soc. Dalton Trans.* **1993**, 2977.
[40] D. R. Gamelin, M. W. George, P. Glyn, F.-W. Grevels, F. P. A. Johnson, W. Klotzbücher, S. L. Morrison, G. Russell, K. Schaffner, J. J. Turner, *Inorg. Chem.* **1994**, *33*, 3246.
[41] A. Vlček, Jr., *Top. Organomet. Chem.* **2010**, *29*, 73.
[42] A. Vlček, Jr., S. Záliš, *Coord. Chem. Rev.* **2007**, *251*, 258.
[43] D. J. Liard, M. Busby, P. Matousek, M. Towrie, A. Vlček, Jr., *J. Phys. Chem. A* **2004**, *108*, 2363.
[44] J. E. Hansen, J. W. Longworth, G. R. Fleming, *Biochemistry* **1990**, *29*, 7329.
[45] E. Wolcan, J. L. Alessandrini, M. R. Féliz, *J. Phys. Chem. B* **2005**, *109*, 22890.
[46] T. E. Knight, J. K. McCusker, *J. Am. Chem. Soc.* **2010**, *132*, 2208–2221.
[47] F. P. A. Johnson, M. W. George, F. Hartl, J. J. Turner, *Organometallics* **1996**, *15*, 3374.
[48] A. Gabrielsson, F. Hartl, H. Zhang, J. R. Lindsay Smith, M. Towrie, A. Vlček, Jr., R. N. Perutz, *J. Am. Chem. Soc.* **2006**, *128*, 4253.
[49] G. J. Stor, F. Hartl, J. W. M. van Outersterp, D. J. Stufkens, *Organometallics* **1995**, *14*, 1115.
[50] J. D. Lewis, M. Towrie, J. N. Moore, *J. Phys. Chem. A* **2008**, *112*, 3852.
[51] A. M. Blanco-Rodríguez, M. Towrie, J. Sýkora, S. Záliš, A. Vlček, Jr., unpublished results.
[52] K. Brettel, C. Aubert, M. H. Vos, P. Mathis, A. P. M. Eker, *Nature* **2000**, *405*, 586.
[53] A. El Nahhas, C. Consani, A. M. Blanco-Rodríguez, K. M. Lancaster, O. Braem, A. Cannizzo, M. Towrie, I. P. Clark, S. Záliš, M. Chergui, A. Vlček, Jr., *Inorg. Chem.* **2011**, DOI: 10.1021/ic102324p.
[54] A. Harriman, *J. Phys. Chem.* **1987**, *91*, 6102.
[55] A. Lukacs, A. P. M. Eker, M. Byrdin, K. Brettel, M. H. Vos, *J. Am. Chem. Soc.* **2008**, *130*, 14394.
[56] M. Byrdin, A. P. M. Eker, M. H. Vos, K. Brettel, *Proc. Natl. Acad. Sci. USA* **2003**, *100*, 8676–8681.
[57] M. Byrdin, A. Lukacs, V. Thiagarajan, A. P. M. Eker, K. Brettel, M. H. Vos, *J. Phys. Chem. A* **2010**, *114*, 3207–3214.
[58] A. Lukacs, A. P. M. Eker, M. Byrdin, S. Villette, J. Pan, K. Brettel, M. H. Vos, *J. Phys. Chem. B* **2006**, *110*, 15654.
[59] F. Tanaka, H. Chosrowjan, S. Taniguchi, N. Mataga, K. Sato, Y. Nishina, K. Kiyoshi Shiga, *J. Phys. Chem. B* **2007**, *111*, 5694.
[60] H.-W. Park, S.-T. Kim, A. Sancar, J. Deisenhofer, *Science* **1995**, *268*, 1866.
[61] E. W. Debler, G. F. Kaufmann, M. M. Meijler, A. Heine, J. M. Mee, G. Pljevaljcic, A. J. Di Bilio, P. G. Schultz, D. P. Millar, K. D. Janda, I. A. Wilson, H. B. Gray, R. A. Lerner, *Science* **2008**, *319*, 1232.
[62] J. L. Seifert, T. D. Pfister, J. M. Nocek, Y. Lu, B. M. Hoffman, *J. Am. Chem. Soc.* **2005**, *127*, 5750.
[63] S. A. Kang, B. R. Crane, *Proc. Natl. Acad. Sci. USA* **2005**, *102*, 15465–15470.

Received: July 28, 2010
Revised: December 12, 2010
Published online: April 5, 2011

